In vivo quantitative proteomics of somatosensory cortical synapses shows which protein levels are modulated by sensory deprivation

Margaret T. Butko[a,1], Jeffrey N. Savas[b,1], Beth Friedman[a], Claire Delahunty[b], Ford Ebner[c], John R. Yates III[b,2], and Roger Y. Tsien[a,d,2]

[a]Department of Pharmacology and [d]Howard Hughes Medical Institute, University of California at San Diego, La Jolla, CA 92093; [b]Department of Chemical Physiology, The Scripps Research Institute, La Jolla, CA 92037; and [c]Department of Psychology, Vanderbilt University, Nashville, TN 37240

Contributed by Roger Y. Tsien, January 9, 2013 (sent for review December 4, 2012)

Postnatal bilateral whisker trimming was used as a model system to test how synaptic proteomes are altered in barrel cortex by sensory deprivation during synaptogenesis. Using quantitative mass spectrometry, we quantified more than 7,000 synaptic proteins and identified 89 significantly reduced and 161 significantly elevated proteins in sensory-deprived synapses, 22 of which were validated by immunoblotting. More than 95% of quantified proteins, including abundant synaptic proteins such as PSD-95 and gephyrin, exhibited no significant difference under high- and low-activity rearing conditions, suggesting no tissue-wide changes in excitatory or inhibitory synaptic density. In contrast, several proteins that promote mature spine morphology and synaptic strength, such as excitatory glutamate receptors and known accessory factors, were reduced significantly in deprived synapses. Immunohistochemistry revealed that the reduction in SynGAP1, a postsynaptic scaffolding protein, was restricted largely to layer I of barrel cortex in sensory-deprived rats. In addition, protein-degradation machinery such as proteasome subunits, E2 ligases, and E3 ligases, accumulated significantly in deprived synapses, suggesting targeted synaptic protein degradation under sensory deprivation. Importantly, this screen identified synaptic proteins whose levels were affected by sensory deprivation but whose synaptic roles have not yet been characterized in mammalian neurons. These data demonstrate the feasibility of defining synaptic proteomes under different sensory rearing conditions and could be applied to elucidate further molecular mechanisms of sensory development.

mass spectrometric proteomics | somatosensory cortex | experience-dependent plasticity | synaptic protein dynamics

Sensory information is encoded in the brain by activation of specific neuronal circuits that operate via chemical synapses. Important sensory experiences are stored by strengthening activated synapses in the circuit, a process known as "experience-dependent plasticity" (1). When animals are deprived of sensory experience during development, for example, by trimming rodent whiskers from birth to 30 d after birth, synaptic strength and mature synaptic morphology are attenuated, suggesting that the low activity in the deprived circuits interferes with normal development (2–7). However, the molecular changes that alter these synaptic properties in response to experience remain unclear. Synaptic activation has been shown to promote regulated and highly localized effects on synaptic proteins such as local translation, recruitment, and targeted degradation (8–11), and this spatiotemporal control of protein availability is required for long-term plasticity and synaptic maturation, which are fundamental in memory formation and storage and ultimately for an organism's survival (12–14). The need for highly controlled protein availability is highlighted in studies of neurological diseases, which often result from the disruption of protein availability at the synapse (15–17). Therefore, it is clear that local synaptic protein dynamics are critical for promoting changes in synaptic morphology and strength to stabilize the structure appropriate to the activation levels; however, it remains unclear which synaptic proteins are critical for endowing these synaptic properties.

The present study used quantitative MS-based proteomics to search for synaptic proteins whose levels are affected by sensory deprivation during development. To generate synaptosome samples under conditions of different synaptic input levels, we isolated synaptosomes from barrel cortex in mice that had undergone daily bilateral whisker trimming (sensory-deprived mice) or whisker brushing (sensory-normal mice) from postnatal day (P)4–P30. The murine vibrissa trigeminal system offers several advantages for studying changes in synaptic properties caused by enhanced or suppressed sensory experiences. First, sensory experience can be manipulated without physical damage to peripheral sensory axons so that any effects can be ascribed to changes in neuronal activation. Second, primary somatosensory (S1) cortex can be localized anatomically on the basis of surface vasculature, and its distinct barrel cytoarchitecture can be distinguished easily in cortical tissue samples (4, 18). Third, vibrissa function is critical to rodent navigation through environments, and there is a rich literature that documents structural and functional effects of varied sensory experience on cortical development (1, 3, 5, 6). Although a proteomics study of crude synaptosomes may be ambitious because of the heterogeneity of both barrel cortex tissue and synaptic

Significance

We applied quantitative mass spectrometry to define how sensory experience alters the synaptic proteome in primary sensory cortex. Our results demonstrate that sensory deprivation reduced proteins implicated in spine enlargement and synaptic strength and increased protein-degradation machinery at synapses. Importantly, we identified novel synaptic proteins whose levels were affected by sensory deprivation but whose synaptic roles have not yet been characterized in mammalian neurons. Thus, this study provides a crucial starting point for numerous investigations of the molecular basis for synaptic modulation and demonstrates the feasibility of using this method to define synaptic proteomes under different sensory rearing conditions.

Author contributions: M.T.B., J.N.S., B.F., F.E., J.R.Y., and R.Y.T. designed research; M.T.B., J.N.S., B.F., and C.D. performed research; J.N.S. and J.R.Y. contributed new reagents/analytic tools; M.T.B., J.N.S., and B.F. analyzed data; and M.T.B., J.N.S., B.F., and R.Y.T. wrote the paper.

The authors declare no conflict of interest.

Freely available online through the PNAS open access option.

Data deposition: Data reported in this paper are available at http://fields.scripps.edu/published/whisker/.

[1]M.T.B. and J.N.S. contributed equally to this work.

[2]To whom correspondence may be addressed. E-mail: jyates@scripps.edu or rtsien@ucsd.edu.

This article contains supporting information online at www.pnas.org/lookup/suppl/doi:10.1073/pnas.1300424110/-/DCSupplemental.

structure, we predict that our approach can reveal regulated proteins with confidence.

In this study, barrel cortex synaptosomes from ^{15}N-enriched mice served as internal standards for direct comparison of the experimental groups. ^{15}N labeling of rodents facilitates accurate, proteome-wide quantitative analysis of long-lived proteins and synapse-wide changes during development (19–21). Out of more than 7,000 quantified proteins, we identified 89 significantly reduced and 161 significantly elevated proteins in sensory-deprived synapses, and we validated 22 of these proteins by immunoblotting and one by immunohistochemistry. Proteins that were significantly down-regulated in sensory-deprived animals may represent the most attractive candidates for degrading synaptic properties such as synaptic strength and spine maturity in synapses receiving reduced input activity. Postsynaptic proteins that promote spine enlargement and synaptic strength, two characteristics that promote synaptic maturation and stability, also are of great interest. Importantly, we identified many less-characterized synaptic proteins that were altered by sensory experience, and this dataset will provide interesting future targets for understanding the molecular basis of mammalian experience-dependent plasticity.

Results

We set out to identify the synaptic proteins regulated by developmental sensory experience in mouse barrel cortex using quantitative 2D liquid chromatography and tandem mass spectrometry (LCLC-MS/MS). The synapses influenced by sensory deprivation are thought to be newly formed synapses that fail to become strong and stable. We reduced activity in barrel cortex by trimming all whiskers daily from P4, near the beginning of synaptogenesis, to P30, well after the critical window for synaptic plasticity (4, 22), to produce barrel cortex synapses that develop under low-activity (sensory-deprived) conditions (Fig. 1*A*). In a second, sensory-normal group of animals, all whiskers were brushed daily to control for animal handling during whisker manipulation (Fig. 1*A*). To ensure broad synaptic proteome coverage, we prepared barrel cortex synaptosome fractions for analysis. The reduced level of complexity of synaptosomes allows the LCLC-MS/MS method to analyze nearly all proteins present in the sample (23). We used a third group of animals, sensory-normal mice labeled by ^{15}N (Fig. 1*A*), as an internal standard and performed relative protein quantitation for each MS run using a ratio-of-ratios approach (24).

Barrel cortex tissue was isolated from whole cortex using a tissue puncher. The punched tissue was considered acceptable for use in the study if the remaining cresyl-violet–stained cortex contained few large sensory barrels around the punch and mostly small barrels that receive input from small nasal whiskers rostral to the punch (Fig. 1*B*). Coronal sections through an acceptable punched barrel cortex sample indicated that the cortical layer architecture imaged by cresyl violet (Fig. 1*C*, *Left*) and the barrel architecture imaged by immunostaining for a glutamate transporter (VGlut2; Fig. 1*C*, *Right*) remained intact in the punched tissue. Homogenates from acceptable punched barrel cortex samples were mixed 1:1 (^{14}N/ ^{15}N) early in the work flow to minimize any potential bias introduced during synaptosome preparation, sample processing, or MS analysis. Three biological replicates from three different mice were generated for the trimmed and the brushed experimental groups. Synaptosomes prepared from barrel cortex demonstrated enrichment for synaptic proteins by immunoblotting and preservation of both presynaptic and postsynaptic structures by electron microscopy (Fig. 1*D*).

In each synaptosome sample we identified ~3,500 proteins from ~35,000 peptides at a protein false-discovery rate (FDR) <1%. The total number of proteins identified throughout all samples was 7,134 proteins from 60,962 total peptides. We then quantified about 75% of the identified peptides based on confidence measurements (see *Analysis of Tandem Mass Spectra* section in *Materials and Methods* for details). Proteins of interest were identified by first generating a ^{14}N-trim/^{15}N-brush (trimmed) or ^{14}N-brush/^{15}N-brush (brushed) ratio to generate a final ^{14}N-trim/^{14}N-brush "ratio of ratios" (Fig. 2*A*). We compared the three "trimmed" with the three "brushed" datasets to calculate fold change and significance by ANOVA analysis and graphed these results as a volcano plot (Fig. 2*B*). Eighty-nine proteins

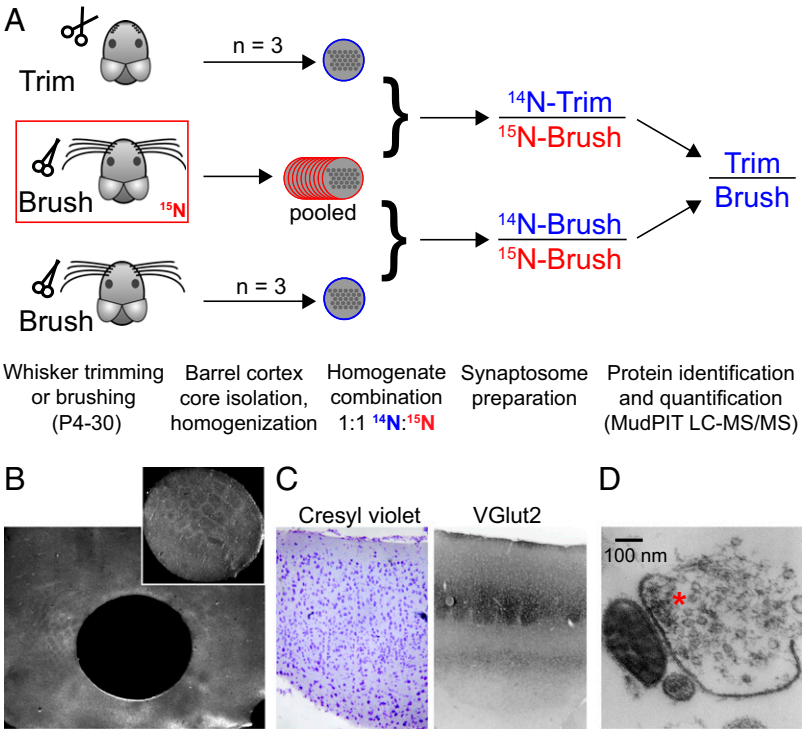

Fig. 1. Method used to isolate synapses after normal and reduced input activity in the barrel cortex during postnatal development. (*A*) Experimental scheme for identifying and quantifying proteins up- or down-regulated in sensory-deprived compared with sensory-normal barrel cortices (blue) by LCLC-MS/MS using ^{15}N mice (red) as an internal standard. (*B*) Image of a 100-μm-thick tangential section of punched cortex showing the location of a barrel punch with the resulting absence of large barrel architecture in the surrounding cortex, which would identify the corresponding punch as acceptable for inclusion in the experiment. (*Inset*) A 100-μm-thick section of the corresponding barrel punch containing many large barrel structures. (*C*) Coronal section of an acceptable punched barrel cortex sample imaged by cresyl violet to verify intact columnar cortical cytoarchitecture (*Left*) and by immunoreactivity for the glutamate transporter (VGlut2) to outline the barrel structures (*Right*). (*D*) Electron micrograph of a synaptosome preparation demonstrating the presence of presynaptic (red asterisk marks a cluster of synaptic vesicles) and postsynaptic structures.

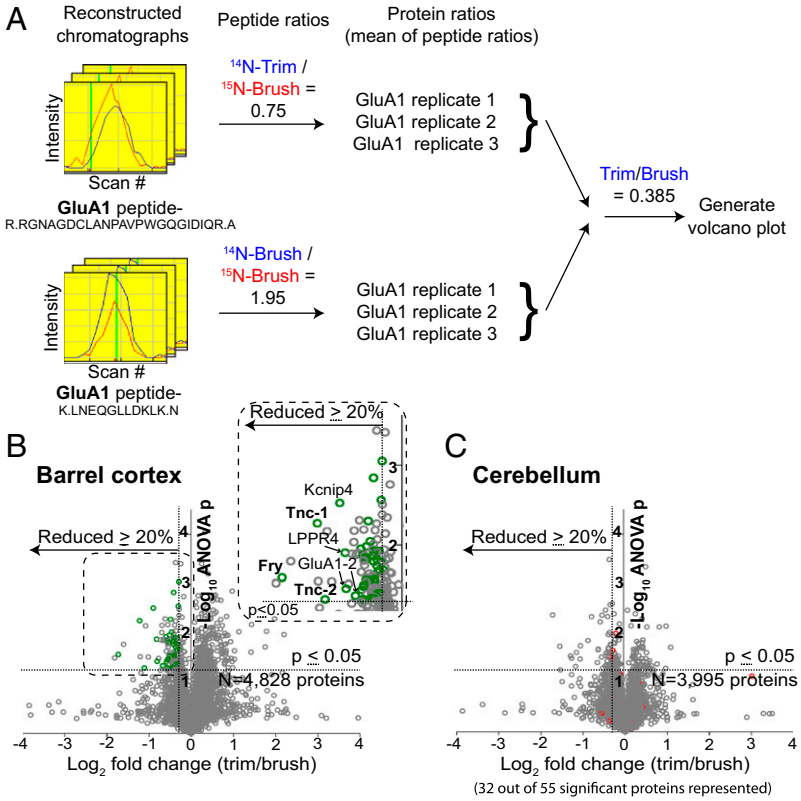

Fig. 2. Quantification method for synaptic proteins in sensory-deprived and sensory-normal synapses. (*A*) Schematic for quantifying protein levels by LCLC-MS/MS using GluA1 as an example. Reconstructed peptide chromatographs containing both ^{14}N and ^{15}N species were used to calculate trim/brush (trimmed, *Upper*) or brush/brush (brushed, *Lower*) ratios. Protein ratios are generated from mean peptide ratios for each biological replicate. The mean protein ratio over all three biological replicates was used to generate a final trim/brush ratio of ratios. The indicated result is a single biological replicate. (*B*) Volcano plot of the complete identified and quantified protein cohort from barrel cortex synaptosomes by LCLC-MS/MS, graphed as Log2 fold change trim/brush vs. -Log10 ANOVA *P* value. (*Inset*) Proteins that satisfied both the statistical cutoff (ANOVA $P < 0.05$) and were reduced by ≥20% in deprived synapses are shown as unlabeled points (>1.2-fold reduced), in regular text (>1.5-fold reduced), or in bold text (>2.0-fold reduced). Significantly reduced synaptic proteins are represented by green points. (*C*) Volcano plot of all proteins quantified from whole-cerebellum synaptosomes by LCLC-MS/MS with the statistical cutoff (ANOVA $P < 0.05$) and ≥20% reduction cutoff shown. Synaptic proteins that were significantly reduced in sensory-deprived barrel cortex synapses (green points in *B*, listed in Table 1) are indicated as red data points. Note that 32 of the 55 synaptic proteins that were significantly reduced in barrel cortex (Table 1) also were identified in cerebellum, and only one was significantly reduced in cerebellum also.

were significantly reduced (Table S1), and 161 proteins were significantly elevated (Table S2) by at least 1.2-fold in trimmed with respect to brushed samples. Of these, only a few were altered by more than 1.5-fold (nonbold text in Fig. 2*B Inset* and light gray fill in Table 1) or by 2.0-fold (bold text in Fig. 2*B Inset* and dark gray fill in Table 1). Here, we focus our analysis on the synaptic proteins that were significantly down-regulated in sensory-deprived animals, suggesting their enrichment by normal activity in stable synapses (green points in Fig. 2*B Inset*, Table 1, and bold text in Table S1, *Left Column*). Table 1 lists synaptic proteins that were significantly reduced in deprived synapses, grouped by subsynaptic location, and reports their corresponding International Protein Index (IPI) number, ratio of average trimmed:brushed protein levels (T/B), number of quantified peptides ($^{14}N/^{15}N$ pairs) from which the average was calculated, ANOVA *P* value, and previous studies that have demonstrated the effects of down-regulation or up-regulation of the protein on spine morphology, neurite morphology, synaptic transmission, and/or behavior.

Of the 250 proteins that exhibited significant differences (up or down) between barrel synaptosomes in trimmed and brushed mice, only four also were changed significantly in whole-cerebellum synaptosomes (Tables S1 and S2, light gray fill), indicating that these reported changes demonstrated a high level of specificity for the barrel cortex. Cerebellum results were graphed as a volcano plot, and synaptic proteins listed in Table 1 are indicated as red points in the graph (Fig. 2*C*). Notably, only one protein (GluA1) in Table 1 also was reduced significantly in cerebellum, and it was reduced by a lesser extent in cerebellum than in barrel cortex. To verify the MS data with an independent technique, semiquantitative immunoblotting was performed with 22 antibodies that recognized distinct bands at the predicted molecular weight using β-actin staining for normalization (Fig. 3). All 22 immunoassays reported protein levels in trimmed vs. brushed samples (19 decreased, 2 unchanged, and 1 increased in trimmed) in concordance with the MS data, thereby indicating few false-positive identifications.

In intact brain, synaptic protein expression is not limited to synapses, because these proteins are synthesized and trafficked throughout the neuron, and experience-dependent alterations in the laminar localization of synaptic proteins in intact cortex rarely have been observed (67). Therefore, we tested whether the quantitative alternation in synaptic protein expression could translate to altered spatial localization in intact brain. We compared SynGAP1 protein distribution between sensory-deprived (trimmed) and sensory-normal (brushed) barrel cortex sections (Fig. 4). SynGAP1 is a postsynaptic density protein that exhibits nearly equimolar abundance in forebrain as PSD-95 (68), and loss of SynGAP1 through targeted mutation is deleterious to barrel cortex formation during development (69) and results in learning deficits (59, 70). Furthermore, SynGAP1 mRNA has been shown previously to be spatially concentrated in layers II and V of P35 mice (69). In sensory-normal (brushed) barrel cortex, SynGAP1 protein immunoreactivity was concentrated in layer I, whereas layers II–VI were stained diffusely except for faint delineation of cortical barrels in layer IV and slightly higher staining in layer Va (Fig. 4*B*). Despite the high level of mRNA expression in neuronal soma demonstrated previously (69), neuronal soma generally were poor in SynGAP1 protein immunoreactivity with only scattered SynGAP1-positive neuronal soma visible in layer V. Sensory-deprived (trimmed) barrel cortex also showed diffuse staining in layers II–VI; however the high SynGAP1 immunoreactivity in layer I was not observed in sensory-deprived cortex (Fig. 4*A*). When SynGAP1 staining was represented as a ratio of layer I (Fig. 4*C*) to layer IV (defined by VGlut2 immunoreactivity of barrel afferents; Fig. 4*D*), this ratio was significantly higher in sensory-normal barrel cortex (Fig. 4*E*). These data indicate that the significant reductions in protein expression detected in sensory-deprived synapses by proteomics and immunoblotting

Table 1. Synaptic proteins significantly reduced in sensory-deprived barrel cortex

Protein	T/B (%)	*P*	Average $^{14}N/^{15}N$ pairs	Up/down-regulation at the synapse	IPI
Membrane-bound					
Fry	30	0.026	2	(25)*	IPI00655161.6
KChIP4	54	0.003	2	(26)†	IPI00621710.2
LPPR4	57	0.013	10	(27)†,‡	IPI00420590.3
GluA1	57	0.035	15	(28)†,‡	IPI00407939.1
Slc4a7	62	0.009	7	(29)‡	IPI00664442.3
GluN1	63	0.013	14	(30)†,§	IPI00755015.1
TARP-γ3	67	0.036	5	(31)†	IPI00122300.1
LPPR2	67	0.048	4		IPI00222105.1
Pcdh1	68	0.014	13		IPI00719927.2
GIRK1	68	0.032	4	(32)‡	IPI00119615.1
Teneurin-2	69	0.018	9	(33)§	IPI00123782.6
Robo1	69	0.049	2	(34)*	IPI00130664.5
Icam5	69	0.015	13	(35)§	IPI00877299.1
GIRK2	70	0.015	3	(32)‡	IPI00227086.2
Gprin1	70	0.028	25	(36)*	IPI00138232.4
GluA2	70	0.049	28	(37)†,‡,§	IPI00608015.1
Cpne6	70	0.041	14		IPI00927968.1
GluN2B	70	0.028	27	(38)†,‡	IPI00321320.3
Flotillin-2	74	0.024	6		IPI00754549.1
Dpp6	75	0.014	20	(39)†	IPI00880742.1
Cacn-β1	75	0.001	5	(40)†	IPI00321850.3
Gng2	76	0.026	6		IPI00230194.5
Rab35	76	0.027	5	(41)*	IPI00130489.1
GABAA-α2	77	0.034	5	(42)*	IPI00110598.1
GluN2A	78	0.012	21	(43)†	IPI00118380.2
Plexin-A1	78	0.041	18	(44)*	IPI00137311.1
Gnaq	78	0.009	16	(45)‡	IPI00228618.5
Flotillin-1	79	0.021	10	(46)*,†,§	IPI00117181.1
Slc8a2	79	0.044	20	(47)†,‡	IPI00170310.1
Lphn 3	79	0.040	6	(48)‡,§	IPI00619988.3
Camk-v	79	0.012	18		IPI00122486.3
KCNN2	81	0.026	2	(49)†,‡	IPI00467814.2
Adcy9	82	0.001	12		IPI00313750.3
Slc6a7	82	0.044	3		IPI00420909.1
ECM					
Tnc	43	0.005	7	(50)†,‡	IPI00403938.2
Annexin-2	68	0.033	1	(51)*	IPI00468203.3
Glypican1	75	0.012	8		IPI00137336.1
Hapln4	78	0.015	4		IPI00229184.3
Intracellular					
Rgs12	47	0.007	1	(52)*	IPI00229481.2
Bad	62	0.007	1	(53)†	IPI00119986.1
GKAP	66	0.011	7	(54)§	IPI00136402.2
Prickle2	68	0.016	7	(55)*	IPI00349970.6
Ptk2b	72	0.023	10	(56)†	IPI00133132.1
Kalirin	73	0.009	18	(57)*,†,‡,§	IPI00848608.1
Map4	73	0.028	15		IPI00406741.5
Shank1	73	0.047	20	(58)†,‡,§	IPI00758339.1
SynGAP1	75	0.028	53	(59)†,‡,§	IPI00663736.2
Catenin-α2	76	0.024	30	(60)*,‡,§	IPI00119870.2
PKCγ	76	0.007	24	(61)†,‡	IPI00122069.1
Translin	77	0.044	3	(62)‡	IPI00124684.1
Rgs14	77	0.005	4	(63)†,‡	IPI00125649.1
Sap102	80	0.021	30	(64, 65)†,‡,§	IPI00623890.1
Catenin-β1	81	0.016	26	(60)*,†,‡,§	IPI00125899.1
Catenin-δ2	81	0.042	17	(60)*,†,‡,§	IPI00136135.1
Map2	81	0.003	55		IPI00118075.1
Arp2	83	0.021	12	(66)*	IPI00177038.1

Proteins are grouped by subsynaptic location with their corresponding IPI number. The ratio of average trimmed:brushed protein levels (T/B), number of quantified peptides ($^{14}N/^{15}N$ pairs) from which the average was calculated, and ANOVA *P* value for each protein are indicated. Light gray fill indicates proteins altered by more than 1.5-fold. Dark gray fill indicates proteins altered by more than 2.0-fold.
*Study demonstrates the effects of down-regulation or up-regulation of protein on neurite morphology.
†Study demonstrates the effects of down-regulation or up-regulation of protein on synaptic transmission.
‡Study demonstrates the effects of down-regulation or up-regulation of protein on behavior.
§Study demonstrates the effects of down-regulation or up-regulation of protein on spine morphology.

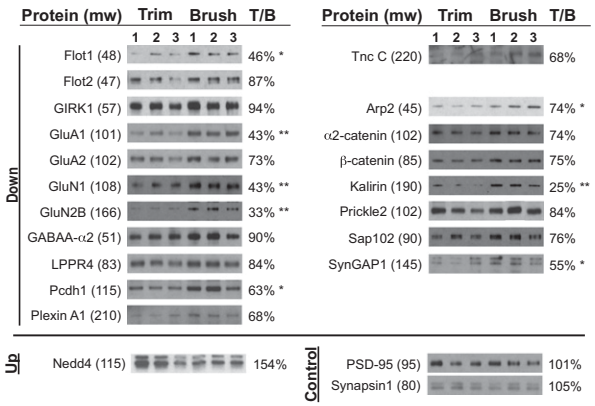

Fig. 3. Immunochemical analysis verified changes predicted by the MS results. Western blots of all six barrel cortex samples (three trimmed and three brushed) probed for 19 proteins identified by MS as significantly reduced (Down), two proteins identified as unchanged (Control), and one protein identified as elevated (Up) in trimmed vs. brushed barrel cortex samples. The optical density for each band was calculated and normalized to β-actin immunoreactivity, and then the ratio of the average normalized optical density for trimmed vs. brushed (T/B) was calculated. Lower percentages indicate greater reduction as a result of trimming (*$P < 0.05$., **$P < 0.01$).

translated to the intact cortex as a change in the laminar expression of this synaptic protein.

One notable class of proteins that was accumulated significantly in deprived synapses was the protein-degradation machinery (Table 2 and bold text in Table S2, *Left Column*), including proteasome subunits (Psmb7, Psmd1, and Psmd11), E2 ligases (Ube2o and Ube2l3), and E3 ligases (Ubr4 and Nedd4). Table 2 lists proteasome proteins that were significantly elevated in deprived synapses and reports their corresponding IPI number, ratio of average trimmed:brushed protein levels (T/B), number of quantified peptides ($^{14}N/^{15}N$ pairs) from which the average was calculated, ANOVA *P* value, and previous studies that have demonstrated the effects of down-regulation or up-regulation of the protein on spine morphology, neurite morphology, synaptic transmission, and/or behavior.

Discussion

Previous attempts to identify and characterize key synaptic proteins that endow synaptic stability have relied heavily on up-regulation or down-regulation of individual candidates to estimate effects on synaptic strength or maturity. The idea of an unbiased search for proteins up-regulated as a result of sensory stimulation is not new, but previous attempts based on ex vivo radiolabeling analyzed by gel electrophoresis (73) were handicapped by low sensitivity, low resolution, and inability to identify the molecules showing alterations. Heavy-stable isotopic labeling with MS-based identification and quantification (74) has provided a powerful and nearly unbiased strategy for identifying proteins that are enriched in activated synapses in vitro. Now stable isotopic labeling of amino acids in mammals (SILAM) is demonstrated (75), and this method is essential for investigating synaptic protein responses to experience-dependent plasticity in vivo. The sensitivity of current MS-based techniques still requires sampling an entire heterogeneous brain region instead of a single cell or synapse (76). Therefore, the challenge in identifying synaptic proteins that endow synaptic stability by MS-based proteomics is the availability of whole-tissue samples that can be manipulated before analysis.

It is well established that diminishing sensory activity in particular regions of the brain during synaptogenesis and maturation can alter synaptic properties drastically throughout that tissue. Indeed, whisker trimming is widely used to reduce sensory input to the barrel cortex, and previously this technique was shown to affect synaptic morphology and transmission in this tissue (77, 78). Using quantitative MS-based techniques and using ^{15}N mice as an internal standard, synaptic protein profiles of barrel cortex in sensory-deprived mice that had undergone daily bilateral whisker trimming were compared with profiles in sensory-normal mice receiving bilateral whisker brushing. Results from this in vivo proteomics screen were used to search for synaptic proteins that were reduced in deprived vs. normal synapses, thereby predicting enrichment in stable synapses that receive normal sensory input. We identified proteins that were both up- (161 proteins) and down- (89 proteins) regulated in sensory-deprived synapses and verified 20 of these proteins by immunochemistry (Figs. 3 and 4), thereby supporting the conclusion that the MS data are accurate. As expected, synaptosome samples contained proteins from both excitatory and inhibitory synapses, such as glutamate and GABA receptors, respectively (Table 1), thereby indicating the inclusion of both classes of synapses in our analysis. We focus our discussion on the synaptic proteins that were significantly down-regulated in sensory-deprived animals (Fig. 2*B*, *Inset* and Table 1), suggesting their activity-based enrichment in stable synapses.

More than 95% of quantified proteins, including abundant synaptic proteins such as PSD-95 and gephyrin, exhibited no significant difference under high- and low-activity rearing conditions, suggesting no tissue-wide changes in excitatory or inhibitory synaptic density. Synaptic proteins that were reduced significantly in deprived barrel cortex synapses (Table 1) represent several classes of synaptic proteins, such as receptors, channels, transmembrane,

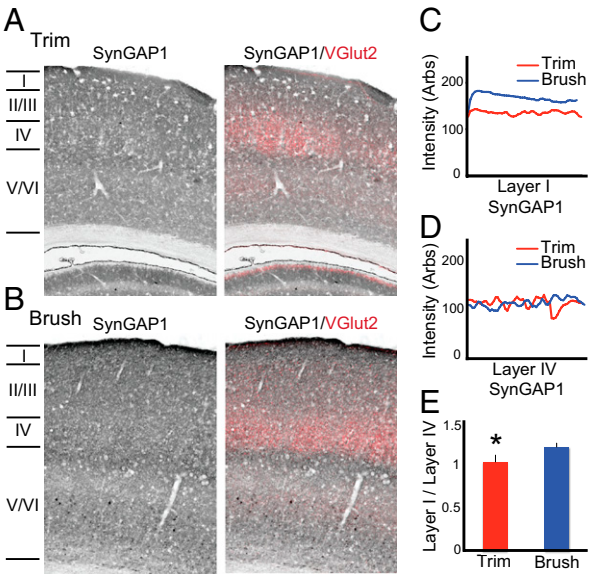

Fig. 4. SynGAP1 protein distribution differs in coronal sections from sensory-deprived (trimmed) and sensory-normal (brushed) barrel cortex. (*A* and *B*) Immunohistochemistry of whole-hemisphere brain sections through cortex from a representative trimmed (*A*) and brushed (*B*) barrel field stained for SynGAP1 alone (*Left*) and overlaid with VGlut2 staining to mark layer IV (red fluorescence) (*Right*). (*C* and *D*) SynGAP1 immunoreactivity in sections from *A* (trimmed, red) and *B* (brushed, blue) was graphed as a function of cortical depth through layer I (*C*) and layer IV (*D*). (*E*) The ratio of total layer I to layer IV SynGAP1 staining was reduced significantly in sensory-deprived (trimmed) vs. sensory-normal (brushed) barrel cortex ($P = 0.012$, two-tailed paired *t* test, $n = 4$ animals per condition). Total layer I to layer IV SynGAP1 immunoreactivity ratios were calculated by dividing the average immunoreactivity across layer I by the average immunoreactivity across layer IV for a given tissue section, and these values were averaged across four animals per condition. This representation of the staining ratio provides an internal normalization so that staining in different sections can be compared. SynGAP1 immunoreactivity across all cortical layers for all animals represented here is graphed in Fig. S1.

Table 2. Proteasomal proteins significantly up-regulated in sensory-deprived barrel cortex synapses

Proteasomal protein	T/B (%)	*P*	Average $^{14}N/^{15}N$ pairs	Up/down-regulation at the synapse	IPI
Psmb7	144	0.002	4		IPI00136483.1
Psmd1	137	0.039	9		IPI00267295.5
Ubr4	131	0.028	10	(71)*	IPI00845523.1
Ube2o	126	0.038	7		IPI00453803.5
Ube2l3	126	0.015	7		IPI00128760.1
Psmd11	124	0.029	7		IPI00222515.5
Nedd4	122	0.046	3	(72)†	IPI00462445.2

Proteins are grouped by subsynaptic location with their corresponding IPI number. The ratio of average trimmed:brushed protein levels (T/B), number of quantified peptides ($^{14}N/^{15}N$ pairs) from which the average was calculated, and ANOVA *P* value for each protein are indicated.

*Study demonstrated the effects of down-regulation or up-regulation of this protein on neurite morphology.

†Study demonstrated the effects of down-regulation or up-regulation of this protein on spine morphology.

secreted, postsynaptic density, downstream signaling, presynaptic vesicle, and cytoskeletal proteins (Fig. 5). Several proteins that were statistically down-regulated in deprived synapses have been shown previously to promote large, mushroom-shaped spines, which is a defining morphological feature of mature, stable synapses (for references, see Table 1). Among these proteins are many postsynaptic membrane-associated proteins (GluA2, GluN1, Flotillin1, ICAM5, and Teneurin2), postsynaptic density proteins (GKAP, kalirin, Sap102, Shank1, and SynGAP1) that scaffold membrane signals intracellularly, and three unique postsynaptic catenins (α2, β1, and δ2) that link the scaffold to the actin network. Proteins that modulate neurite morphology (for references, see Table 1) and affect behavior or performance in memory tasks in vivo (for references, see Table 1) also were identified as reduced in deprived synapses, although many of these proteins do not show a clear molecular role in synaptic stability. We predict that these less-characterized synaptic proteins will be interesting future targets to elucidate further the molecular dynamics that give rise to synaptic stability.

Many proteins that promote synaptic strength, another key defining feature of mature and stable synapses, were also statistically down-regulated in sensory-deprived synapses (for references, see Table 1). Among these proteins are several excitatory postsynaptic ionotropic glutamate receptors (GluA1, GluA2, GluN1, GluN2A, GluN2B). GluA3 also was identified as down-regulated but did not meet the statistical guidelines. TARP-γ3, a known GluA auxiliary subunit, also was identified in our screen as down-regulated with deprivation. Furthermore, GluA1 exhibited one

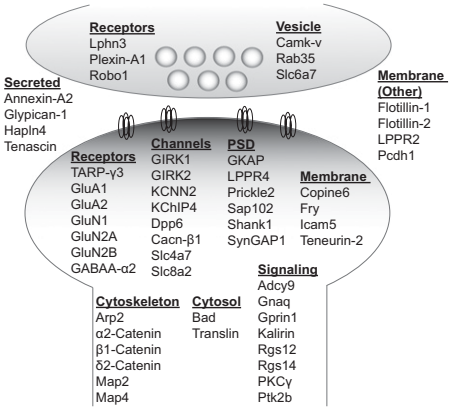

Fig. 5. Summary of the identified pre- or postsynaptic location, protein family, and presumed function of all identified synaptic proteins that were significantly down-regulated in sensory-deprived barrel cortex synapses and listed in Table 1. The effects of sensory deprivation clearly are not restricted to one category of proteins.

of the largest contrasts between sensory-deprived and normal synapses, as expected based on previous reports demonstrating that whisker experiences drive GluA1 into L4 to L2/3 synapses to give rise to experience-dependent synaptic plasticity (79). A GABA receptor (GABAA-α2) also was identified as down-regulated, suggesting that inhibitory synaptic signaling also was affected by sensory deprivation. Although glutamate and GABA receptors were significantly down-regulated in deprived synapses, PSD-95 and gephyrin, the postsynaptic scaffolding proteins in glutamatergic and GABAergic synapses, respectively, remained unchanged, suggesting that these changes were not simply a result of gross changes in glutamatergic and GABAergic synaptic density. However, as suggested previously (77, 78, 80, 81), it is possible that local changes in synaptic density may have been diluted out in our whole-cortex samples. Future studies with different techniques would be required to ascertain to what extent changes in expression result from changes in synapse number vs. changes in expression levels per synapse. Either way, circuitry is altered.

Although most proteins identified as reduced in deprived synapses have been implicated previously in stabilizing synapses, SynGAP1 has been implicated previously in spine elimination, and its down-regulation has been shown to enhance synaptic strength (59). Therefore, we would not have predicted this protein to be reduced in deprived synapses, and we immunostained for this protein in sensory-deprived and normal barrel cortex to determine where this protein exhibited reduced levels. By immunohistochemistry, we demonstrated that sensory deprivation by bilateral whisker trimming altered the laminar distribution of SynGAP1 in the barrel cortex because only layer I barrel cortex exhibited significantly lower SynGAP1 protein levels in sensory-deprived vs. sensory-normal cortex (Fig. 4). These data suggest that the reduction in SynGAP1 protein levels detected by MS and immunoblotting of synaptosomes from whole barrel cortex resulted mostly from reductions in layer I spines. Whisker trimming previously has been shown to reduce spine elimination rates in layer I barrel cortex (82), and that finding is consistent with the reduction in SynGAP1, which is implicated in spine elimination in this region. Because reducing SynGAP1 levels in neurons has been shown previously to stabilize the actin network in spines, leading to activity-independent spine stability (59), our data suggest that layer I spine stabilization as a result of sensory deprivation could be caused, in part, by reduced SynGAP1 protein levels in this region and that these layer I synapses could be stabilized independent of activity levels. Therefore, in addition to its well-characterized role in cognition (83, 84), SynGAP1 appears to play a prominent role in experience-dependent plasticity. Furthermore, the reduction of SynGAP1 in the spines of layer I suggest that SynGAP1 may be an attractive candidate for future in vivo optical imaging studies of somatosensory plasticity. Further investigations to identify the synaptic partners of the layer I spines exhibiting

reduced SynGAP1 levels after sensory deprivation would provide further insight into local organization of sensory information.

We identified many synaptic proteins that have not received attention in the mammalian nervous system but show clear contributions to synapse dynamics in vivo in *Drosophila* or in vitro in neuroblastoma cell lines. For instance, Fry has been shown to be essential for the organization of *Drosophila* sensory neuronal dendrites to cover the entire receptive field without redundancy by avoiding homologous dendritic branches (25). Although Fry expression has been demonstrated in embryonic mammalian brain tissue (85), the role of Fry in mammalian systems has not been studied. Teneurins are required for transsynaptic signaling and organization of the synapse cytoskeleton in *Drosophila* neuromuscular synapses and olfactory receptor neurons (33, 86). Recently, mammalian teneurins have been shown to be latrophilin (Lphn) receptors, which are known to mediate the massive synaptic exocytosis caused by the black widow spider venom α-latrotoxin and which also were identified as reduced in deprived synapses (48, 87). Prickle2 has been shown to regulate neurite formation and outgrowth, but only in neuroblastoma cell lines (55). Further investigations into these proteins in primary mammalian synapses will provide key insights into mechanisms that lead to synaptic maturation and stability.

One notable class of proteins that was accumulated significantly in deprived synapses was the protein-degradation machinery (Table 2), including proteasome subunits (Psmb7, Psmd1, and Psmd11), E2 ligases (Ube2o and Ube2l3), and E3 ligases (Ubr4 and Nedd4). Ubr4 has been shown previously to stabilize neuronal processes by stabilizing microtubules, and knockdown of this protein leads to thin, crooked neurites (71). Nedd4 has been implicated previously in the ubiquitination of GluA1, leading to its internalization and thereby reducing synaptic strength (72, 88). Therefore, the up-regulation of Nedd4 in these deprived synapses may be implicated in the observed reduction in synaptic GluA1 (Table 1), leading to weaker synapses. Up-regulation of the protein-degradation pathway in sensory-deprived synapses suggests that there is greater turnover of synaptic proteins. Together with the data from proteins down-regulated in deprived synapses, these data suggest that sensory deprivation may induce long-term depression at synapses in the barrel cortex, resulting in weaker synapses and higher synapse elimination rates, as suggested previously (89). In the future, localizing these changes in protein-degradation machinery to specific regions and specific cell types could provide valuable insight into how synaptic proteins are regulated during experience-dependent plasticity.

Two popular candidates for protein switches underlying long-term synaptic plasticity are PKMζ and CPEB3, both of which are thought to be self-sustaining once activated to set up a local positive-feedback loop at activated synapses to sustain long-term strength (90, 91). PKMζ, a splice variant of PKCζ, was not detected by MS in barrel cortex synapses in the present study, suggesting that this protein may not be expressed in this region at this age. MS did detect the α, β, γ, δ, δIV, δV, δVI, δVII, ε, θ, and ι isoforms of PKC, of which only PKCγ showed a difference between trimmed and brushed animals (Table 1), suggesting that MS does have enough sensitivity for the related signaling molecules. CPEB3 was elevated significantly in deprived synapses (Table S2). However, because the current MS data do not reveal the activation state of CPEB3 in deprived and normal synapses, it remains ambiguous whether this protein was repressing or activating local protein synthesis in synapses from these two groups of animals. In future MS-based screens, monitoring posttranslational modifications could resolve this ambiguity and find additional molecular differences between deprived and normal synapses.

The results from this proteomics screen are complementary to transcriptome investigations such as the recent unbiased screen for mRNA transcripts enriched in dendrites of the rat hippocampus (92). Protein abundance is affected by both synthesis and turnover and generally cannot be predicted merely from mRNA levels (93). Our search encompassed both pre- and postsynaptic compartments in the barrel cortex, was unbiased with respect to site of protein synthesis, and focused on changes in response to sensory input, whereas the current transcriptome data focus on postsynaptically translatable mRNAs and have not yet included environmental modulation. Nevertheless, the published local transcriptome (92) includes the mRNAs for 229 of our list of 250 proteins significantly modulated by whisker trimming, a remarkable concordance suggesting that most proteins whose abundance depends on synaptic activity are indeed locally translated. Changes in synaptic protein levels have been measured previously in visual cortex in response to sensory deprivation via dark rearing (94), but this screen used a different labeling strategy (iTRAQ), and quantified fewer proteins (467 total). Only 58 of the 250 proteins we identified as altered by sensory deprivation were quantified in this previous screen, and only 11 were significantly altered in visual cortex Also. Of these 11 proteins, only three were altered by more than 1.2-fold, the cutoff used in our study, and all three were altered in the same direction in deprived tissue from both studies, thereby suggesting partial overlap in synaptic proteins that are affected by deprived sensory experience. However, it is possible that the tissue and cell heterogeneity in our whole barrel cortex samples may mask or dilute changes in any particular protein (95).

This unbiased proteomics screen identified changes in the synaptic protein profile resulting from changes in an animal's somatosensory input. As expected, many postsynaptic proteins down-regulated in deprived synapses normally would promote spine enlargement and synaptic strength, two characteristics that promote synaptic stability. Notably, many proteins that are less characterized in regulating synaptic stability but that have been implicated in actin-dependent neurite morphology or in in vivo behavior associated with learning tasks also were down-regulated in sensory-deprived synapses. These proteins are promising future targets for studying synaptic stability. Furthermore, this proteomic screen identified many less-characterized synaptic proteins that show a clear contribution to sensory development and experience-dependent plasticity. Therefore, the present study provides a plethora of good candidates for powerful new techniques to monitor the synthesis and turnover of individual genetically tagged proteins with high spatial and temporal resolution (96–98). Also, overexpression or down-regulation of individual proteins will be required to dissect their functional roles. Thus, this study provides a crucial starting point for innumerable investigations of the molecular basis for synaptic modulation.

The raw files and complete parameter files will be publicly available at http://fields.scripps.edu/published/whisker/ upon publication.

Materials and Methods

Animals. Eight adult FVB mice and 40 of their offspring were used in these studies. All animal procedures were approved by Institutional Animal Care and Use Committee of the University of California, San Diego. To ensure nearly complete SILAM, we took a generational labeling approach: FVB female mice were fed a ^{15}N-rich, Spirulina-based diet for 10 wk starting at P21 (99) and through breeding and weaning to produce "heavy" litters in which more than 95% of the protein content in the brain was ^{15}N enriched (100). Heavy offspring underwent daily bilateral brushing of all whiskers from P4–P30. Offspring from mothers fed a normal (^{14}N) diet for 10 wk underwent either daily bilateral whisker brushing or trimming of all whiskers from P4–P30.

Barrel Cortex Isolation and Synaptosome Preparation. Mice were killed at P30 by retroorbital injection of ketamine/midazolam (k/m), which sufficiently preserved brain vasculature for barrel cortex localization. The brain was removed immediately, and the cortex was isolated and flattened and frozen on a cold surface. The cerebellum and trigeminal ganglion were isolated and frozen immediately. Barrel cortex was punched out of frozen, flattened cortex (1.5-mm diameter) according to vasculature landmarks (18), caudal of

the third branch and centered on the fourth branch of the middle cerebral artery. The remaining cortex was fixed in 2% (wt/vol) paraformaldehyde and 30% (wt/vol) sucrose in HBSS (pH 7.4) for at least 3 d, embedded, sectioned tangentially, stained with cresyl violet, and imaged with dark-field optics to identify remaining barrel structures. A barrel punch was considered acceptable if the remaining tissue contained few if any large sensory barrels around the punch but retained the small whisker barrels located rostral of the punch.

^{14}N barrel punches from trimmed (n = 3) and brushed (n = 3) animals were homogenized separately, and ^{15}N barrel punches (n = 10) were homogenized together in 4 mM Hepes, 0.32 M sucrose, and protease inhibitors. Each ^{14}N homogenate (enough for 50 μg protein synaptosomes) was mixed 1:1 with pooled ^{15}N homogenate before they were cleared by centrifugation at 1,000 × g for 10 min (4 °C), and the supernatant and the subsequent resuspended pellet were centrifuged at 10,000 × g for 15 min (4 °C) to collect the crude synaptosome pellet (P2′) for MS.

Solid urea (8 M) was added to synaptosomes (100 μg protein) for LCLC-MS/MS analysis, and extracts were processed with ProteasMAX (Promega) following the manufacturer's instructions. The samples subsequently were reduced by 5 mM Tris(2 carboxyethyl)phosphine at room temperature for 20 min, alkylated in the dark by 10 mM iodoacetamide for 20 min, and digested with Sequencing Grade Modified Trypsin (Promega) overnight at 37 °C, and the reaction was stopped by acidification.

MudPIT and LTQ Velos Orbitrap MS. The protein digest was pressure-loaded into a 250-μm i.d capillary packed with 2.5 cm of 10-μm Jupiter C18 resin (Phenomenex) followed by an additional 2.5 cm of 5-μm Partisphere strong cation exchanger (Whatman). The column was washed with buffer containing 95% (vol/vol) water, 5% (vol/vol) acetonitrile, and 0.1% formic acid. After washing, a 100-μm i.d capillary with a 5-μm pulled tip packed with 15 cm of 4-μm Jupiter C18 resin was attached to the filter union, and the entire split column (desalting column–union–analytical column) was placed inline with an Agilent 1200 quaternary HPLC and analyzed using a modified 11-step separation described previously (101, 102). The buffer solutions used were 5% (vol/vol) acetonitrile/0.1% formic acid (buffer A), 80% (vol/vol) acetonitrile/0.1% formic acid (buffer B), and 500 mM ammonium acetate/5% (vol/vol) acetonitrile/0.1% formic acid (buffer C). Step 1 consisted of a 90-min gradient from 0–100% (vol/vol) buffer B. Steps 2–11 had a similar profile with the following changes: 5 min in 100% (vol/vol) buffer A, 3 min in X% (vol/vol) buffer C, a 10-min gradient from 0 to 15% (vol/vol) buffer B, and a 108-min gradient from 15–100% (vol/vol) buffer B. The 3-min buffer C percentages (X) were 10, 20, 30, 40, 50, 60, 70, 80, 90, and 100% (vol/vol), respectively, for the 11-step analysis. As peptides eluted from the microcapillary column, they were electrosprayed directly into an LTQ Velos Orbitrap mass spectrometer (Thermo Finnigan) with the application of a distal 2.4-kV spray voltage. A cycle of one full-scan mass spectrum (400–1,800 m/z) at a resolution of 60,000 followed by 15 data-dependent MS/MS spectra at a 35% normalized collision energy was repeated continuously throughout each step of the multidimensional separation. Maximum ion accumulation times were set to 500 ms for survey MS scans and to 100 ms for MS2 scans. Charge state rejection was set to omit singly charged ion species and ions for which a charge state could not be determined for MS/MS. Minimal signal for fragmentation was set to 1,000. Dynamic exclusion was enabled with a repeat count of 1, duration of 20.00 s, list size of 300, exclusion duration of 30.00 s, and exclusion mass with high/low of 1.5 m/z. Application of mass spectrometer scan functions and HPLC solvent gradients were controlled by the Xcaliber data system.

Analysis of Tandem Mass Spectra. Protein identification and quantification and analysis were done with Integrated Proteomics Pipeline - IP2 (Integrated Proteomics Applications, Inc., www.integratedproteomics.com/) using ProLuCID, DTASelect2, Census, and QuantCompare. Spectrum raw files were extracted into ms1 and ms2 files from raw files using RawExtract 1.9.9 (http://fields.scripps.edu/downloads.php) (103), and the tandem mass spectra were searched against the European Bioinformatic Institute (IPI) mouse protein database (www.ebi.ac.uk/IPI/IPImouse.html, downloaded on January 1, 2009). To estimate peptide probabilities and FDRs accurately, we used a target/decoy database containing the reversed sequences of all the proteins appended to the target database (104). Tandem mass spectra were matched to sequences using the ProLuCID (105) algorithm with 50 ppm peptide mass tolerance for precursor ions and 400 ppm for fragment ions.

ProLuCID searches were done on an Intel Xeon cluster running under the Linux operating system. The search space included all fully and half-tryptic peptide candidates that fell within the mass tolerance window with no miscleavage constraint. Carbamidomethylation (+57.02146 Da) of cysteine was considered as a static modification.

The validity of peptide/spectrum matches (PSMs) was assessed in DTASelect (106, 107) using two SEQUEST (108)-defined parameters, the cross-correlation score (XCorr), and normalized difference in cross-correlation scores (DeltaCN). The search results were grouped by charge state (+1, +2, +3, and greater than +3) and tryptic status (fully tryptic, half-tryptic, and nontryptic), resulting in 12 distinct subgroups. In each of these subgroups, the distribution of Xcorr, DeltaCN, and DeltaMass values for (*a*) direct and (*b*) decoy database PSMs was obtained; then the direct and decoy subsets were separated by discriminant analysis. Full separation of the direct and decoy PSM subsets is not generally possible; therefore, peptide match probabilities were calculated based on a nonparametric fit of the direct and decoy score distributions. A peptide confidence of 0.95 was set as the minimum threshold. The FDR was calculated as the percentage of reverse decoy PSMs among all the PSMs that passed the confidence threshold. Each protein identified was required to have a minimum of one peptide; however, this peptide had to be an excellent match with an FDR less than 0.001 and at least one excellent peptide match. After this last filtering step, we estimate that both the protein FDRs were below 1% for each sample analysis.

Each dataset was searched twice, once against light and then against heavy protein databases. After the results from SEQUEST were filtered using DTASelect2, ion chromatograms were generated using an updated version of a program previously written in our laboratory (24). This software, called "Census" (109), is available from the authors for individual use and evaluation through an Institutional Software Transfer Agreement (see http://fields.scripps.edu/census for details).

First, the elemental compositions and corresponding isotopic distributions for both the unlabeled and labeled peptides were calculated, and this information then was used to determine the appropriate m/z range from which to extract ion intensities, which included all isotopes with greater than 5% of the calculated isotope cluster base peak abundance. MS1 files were used to generate chromatograms from the m/z range surrounding both the unlabeled and labeled precursor peptides.

Census calculates peptide ion intensity ratios for each pair of extracted ion chromatograms. The heart of the program is a linear least-squares correlation that is used to calculate the ratio (i.e., slope of the line) and closeness of fit [i.e., correlation coefficient (r)] between the data points of the unlabeled and labeled ion chromatograms. Census allows users to filter peptide ratio measurements based on a correlation threshold; the correlation coefficient (values between zero and one) represents the quality of the correlation between the unlabeled and labeled chromatograms and can be used to filter out poor-quality measurements. In this study, only peptide ratios with the coefficient correlation values (r^2) greater than 0.5 were used for further analysis. In addition, Census provides an automated method for detecting and removing statistical outliers. In brief, SDs are calculated for all proteins using their respective peptide ratio measurements. The Grubbs test ($P <$ 0.01) then is applied to remove outlier peptides. The outlier algorithm is used only when more than two peptides are found in the same protein, because the algorithm becomes unreliable for a small number of measurements. Final protein ratios were generated with QuantCompare, which uses Logtwofold change and ANOVA P value to identify regulated significant proteins. For a protein to be considered in our screen, it had to be "plotted" on our volcano scatter plot (Fig. 2 *B* and *C*); The y axis of these volcano plots is the ANOVA P value, which requires each protein to be quantified in at least two of the biological replicates (so we can calculate the variance) for both the trimmed and brushed animals. To show how many measurements our quantitative measures were drawn from, we have provided peptide counts for each protein listed in Tables 1 and 2 and Tables S1 and S2 (see the columns headed "Average ^{14}N/^{15}N pairs").

Immunochemistry. Immunochemistry was carried out to quantify specific proteins present in synaptosome preparations. The following primary antibodies were diluted in Tris-buffered saline with 0.1% Tween-20 (TBST) with 3% (wt/vol) BSA and 0.001% azide: β-actin (1:10,000; GeneTex 124214), Arp2 (1:500; GeneTex 103311), α2-catenin (1:1,000; Abcam AB11347), β1-catenin (1:1,000; BD 610153), Flotillin-1 (1:250; GeneTex 61307), Flotillin-2 (1:500; GeneTex 114411), GABAA-α2 (1:250; GeneTex 82689), GIRK1 (1:500; GeneTex 108745), GluA2 (1:1,000; Millipore MAB397), GluN1 (1:500; GeneTex 62367), GluN2B (1:1,000; BD 610416), Kalirin (1:1,000; Millipore 07–122), LPPR4 (1:1,000; Abcam AB100935), Plexin-A1 (1:250; GeneTex 62196), PSD-95 (1:20,000; NeuroMab 75–028), Sap102 (1:1,000; GeneTex 110289), Synapsin1 (1:2,000; Millipore AB1543), SynGAP1 (1:1,000; GeneTex 62053), Tenascin C (1:500; GeneTex 62552).

The following primary antibodies were diluted in TBST with 1% (wt/vol) milk: GluA1 (1:1,000; Millipore AB1504), Pcdh1 (1:500; GeneTex 114620), and Prickle2 (1:500; GeneTex 110860).

Synaptosomes were lysed in NuPage lithium dodecyl sulfate sample buffer (Invitrogen) with 10% (vol/vol) 2-mercaptoethanol, run on NuPage 4–12% Novex Bis-Tris gel (Invitrogen), transferred onto a PVDF membrane (Invitrogen), blocked with 10% (wt/vol) milk, and incubated in primary antibody overnight at 4 °C. Goat anti-mouse HRP (1:5,000; Cell Signaling 7076) or goat anti-rabbit HRP (1:2,500; Bio-Rad 172–1019) secondary antibodies were applied for 45 min at room temperature before staining by chemiluminescence (SuperSignal West Pico Chemiluminescent Substrate; Thermo Scientific). The optical density for each band was quantified and normalized to the optical density of the β-actin band in that lane. The average of all three normalized trimmed samples was calculated and compared with the average of all three normalized brushed samples for each protein.

Immunohistochemistry. A second cohort of mice (n = 4 brushed, n = 4 trimmed) was killed at P30 and transcardially perfused with saline followed by 2% (wt/vol) paraformaldehyde. Tissue was cryoprotected in buffered 30% (wt/vol) sucrose with 2% (wt/vol) paraformaldehyde, and the left hemisphere was sectioned on a cryostat at 20-μm thickness. Sections were floated in saline onto Trubond 380 slides (EM Sciences). Slides were processed for antigen retrieval in citrate buffer (pH = 6) (Vector) for 6 min in a microwave. Slides then were batch costained with the following two primary antibodies diluted in TBST with 3% (wt/vol) BSA and 0.001% azide: SynGAP1 (1:2,000; GeneTex 62053) and VGlut2 (1:2,000; Millipore AB2251) for 4 d at room temperature. After thorough washing in PBS, slides were batch stained with the following secondary antibodies: ImmPRESS anti-rabbit (peroxidase) polymer detection kit [50% (vol/vol) in PBS-goat serum] (Vector Laboratories) and goat anti-guinea pig Alexa Fluor 594 (1:2,000; Invitrogen). Sections were imaged on a fluorescence scanner (NanoZoomer; Hamamatsu) with transmitted light and Texas Red filter sets to image 3,3′-Diaminobenzidine and Alexa Fluor 594, respectively. Images were background subtracted using corpus callosum white matter as the background. The cortex staining within the barrel field was quantified for eight separate animals using the "plot" function in ImageJ (Fig. S1). The SynGAP1 layer I and IV plot profiles were extracted based on cytoarchitecture and VGlut2 barrel staining, respectively, and average values were calculated across each layer. For each tissue section, the average SynGAP1 staining in layer I was divided by the average SynGAP1 staining in layer IV, and average staining ratios of layer I to layer IV were calculated from four sections (four animals) per condition (n = 8 sections total). This staining ratio quantification provides an internal normalization so that staining in different sections can be compared. Significance was calculated using a paired two-tailed t test ($P < 0.05$).

Electron Microscopy. A fresh synaptosome pellet (5 μL) prepared from whole cortex was prepared for electron microscopy by high-pressure freezing, freeze substitution, embedding in plastic, and sectioning at 80–100 nm according to published methods (110). Sections were imaged at 80 keV using a JEOL 1200 electron microscope.

ACKNOWLEDGMENTS. We thank Joris deWit, Gentry Patrick, David Kleinfeld, and the members of the R.Y.T. and J.R.Y. laboratories for helpful discussion and the Kleinfeld laboratory for use of their sliding microtome. This work was supported by National Institutes of Health (NIH) Grant 4R37NS027177-23 (to R.Y.T.), National Institute of Aging Fellowship F32AG039127 (to J.N.S.); and NIH Grants P41 RR011823, P01 AG031097, and R01 MH067880 (to J.R.Y.). M.T.B. was supported by an NIH Pharmacology Training grant and by the National Science Foundation Graduate Research Fellowship Program. R.Y.T. is an Investigator of the Howard Hughes Medical Institute.

1. Foeller E, Feldman DE (2004) Synaptic basis for developmental plasticity in somatosensory cortex. *Curr Opin Neurobiol* 14(1):89–95.
2. Allen CB, Celikel T, Feldman DE (2003) Long-term depression induced by sensory deprivation during cortical map plasticity in vivo. *Nat Neurosci* 6(3):291–299.
3. Briner A, et al. (2010) Bilateral whisker trimming during early postnatal life impairs dendritic spine development in the mouse somatosensory barrel cortex. *J Comp Neurol* 518(10):1711–1723.
4. Fox K (2002) Anatomical pathways and molecular mechanisms for plasticity in the barrel cortex. *Neuroscience* 111(4):799–814.
5. Rema V, Armstrong-James M, Ebner FF (2003) Experience-dependent plasticity is impaired in adult rat barrel cortex after whiskers are unused in early postnatal life. *J Neurosci* 23(1):358–366.
6. Shepherd GM, Pologruto TA, Svoboda K (2003) Circuit analysis of experience-dependent plasticity in the developing rat barrel cortex. *Neuron* 38(2):277–289.
7. Takahashi T, Svoboda K, Malinow R (2003) Experience strengthening transmission by driving AMPA receptors into synapses. *Science* 299(5612):1585–1588.
8. Aakalu G, Smith WB, Nguyen N, Jiang C, Schuman EM (2001) Dynamic visualization of local protein synthesis in hippocampal neurons. *Neuron* 30(2):489–502.
9. Bramham CR (2008) Local protein synthesis, actin dynamics, and LTP consolidation. *Curr Opin Neurobiol* 18(5):524–531.
10. Frey U, Morris RG (1997) Synaptic tagging and long-term potentiation. *Nature* 385 (6616):533–536.
11. Ho VM, Lee JA, Martin KC (2011) The cell biology of synaptic plasticity. *Science* 334 (6056):623–628.
12. Sutton MA, Schuman EM (2006) Dendritic protein synthesis, synaptic plasticity, and memory. *Cell* 127(1):49–58.
13. Kandel ER (2001) The molecular biology of memory storage: A dialogue between genes and synapses. *Science* 294(5544):1030–1038.
14. Sebeo J, et al. (2009) Requirement for protein synthesis at developing synapses. *J Neurosci* 29(31):9778–9793.
15. Duncan JE, Goldstein LS (2006) The genetics of axonal transport and axonal transport disorders. *PLoS Genet* 2(9):e124.
16. Kelleher RJ, 3rd, Bear MF (2008) The autistic neuron: Troubled translation? *Cell* 135(3):401–406.
17. Rema V, Armstrong-James M, Ebner FF (1998) Experience-dependent plasticity of adult rat S1 cortex requires local NMDA receptor activation. *J Neurosci* 18(23): 10196–10206.
18. Ayata C, et al. (2004) Laser speckle flowmetry for the study of cerebrovascular physiology in normal and ischemic mouse cortex. *J Cereb Blood Flow Metab* 24(7): 744–755.
19. McClatchy DB, Liao L, Lee JH, Park SK, Yates JR, 3rd (2012) Dynamics of subcellular proteomes during brain development. *J Proteome Res* 11(4):2467–2479.
20. McClatchy DB, Liao L, Park SK, Venable JD, Yates JR (2007) Quantification of the synaptosomal proteome of the rat cerebellum during post-natal development. *Genome Res* 17(9):1378–1388.
21. Savas JN, Toyama BH, Xu T, Yates JR, 3rd, Hetzer MW (2012) Extremely long-lived nuclear pore proteins in the rat brain. *Science* 335(6071):942.
22. Bureau I, Shepherd GM, Svoboda K (2004) Precise development of functional and anatomical columns in the neocortex. *Neuron* 42(5):789–801.
23. Savas JN, Stein BD, Wu CC, Yates JR, 3rd (2011) Mass spectrometry accelerates membrane protein analysis. *Trends Biochem Sci* 36(7):388–396.
24. MacCoss MJ, Wu CC, Liu H, Sadygov R, Yates JR, 3rd (2003) A correlation algorithm for the automated quantitative analysis of shotgun proteomics data. *Anal Chem* 75(24):6912–6921.
25. Emoto K, et al. (2004) Control of dendritic branching and tiling by the Tricornered-kinase/Furry signaling pathway in Drosophila sensory neurons. *Cell* 119(2):245–256.
26. Liang P, Chen H, Cui Y, Lei L, Wang K (2010) Functional rescue of Kv4.3 channel tetramerization mutants by KChIP4a. *Biophys J* 98(12):2867–2876.
27. Trimbuch T, et al. (2009) Synaptic PRG-1 modulates excitatory transmission via lipid phosphate-mediated signaling. *Cell* 138(6):1222–1235.
28. Frey MC, Sprengel R, Nevian T (2009) Activity pattern-dependent long-term potentiation in neocortex and hippocampus of GluA1 (GluR-A) subunit-deficient mice. *J Neurosci* 29(17):5587–5596.
29. Majumdar D, Bevensee MO (2010) Na-coupled bicarbonate transporters of the solute carrier 4 family in the nervous system: Function, localization, and relevance to neurologic function. *Neuroscience* 171(4):951–972.
30. Alvarez VA, Ridenour DA, Sabatini BL (2007) Distinct structural and ionotropic roles of NMDA receptors in controlling spine and synapse stability. *J Neurosci* 27(28): 7365–7376.
31. Kott S, Sager C, Tapken D, Werner M, Hollmann M (2009) Comparative analysis of the pharmacology of GluR1 in complex with transmembrane AMPA receptor regulatory proteins gamma2, gamma3, gamma4, and gamma8. *Neuroscience* 158(1): 78–88.
32. Lüscher C, Slesinger PA (2010) Emerging roles for G protein-gated inwardly rectifying potassium (GIRK) channels in health and disease. *Nat Rev Neurosci* 11(5): 301–315.
33. Mosca TJ, Hong W, Dani VS, Favaloro V, Luo L (2012) Trans-synaptic Teneurin signalling in neuromuscular synapse organization and target choice. *Nature* 484(7393):237–241.
34. Hernández-Miranda LR, et al. (2011) Robo1 regulates semaphorin signaling to guide the migration of cortical interneurons through the ventral forebrain. *J Neurosci* 31(16):6174–6187.
35. Matsuno H, et al. (2006) Telencephalin slows spine maturation. *J Neurosci* 26(6): 1776–1786.
36. Ge X, Qiu Y, Loh HH, Law PY (2009) GRIN1 regulates micro-opioid receptor activities by tethering the receptor and G protein in the lipid raft. *J Biol Chem* 284(52): 36521–36534.
37. Medvedev NI, et al. (2008) The glutamate receptor 2 subunit controls post-synaptic density complexity and spine shape in the dentate gyrus. *Eur J Neurosci* 27(2): 315–325.
38. Wang CC, et al. (2011) A critical role for GluN2B-containing NMDA receptors in cortical development and function. *Neuron* 72(5):789–805.
39. Sun W, et al. (2011) DPP6 establishes the A-type K(+) current gradient critical for the regulation of dendritic excitability in CA1 hippocampal neurons. *Neuron* 71(6): 1102–1115.
40. Leroy J, et al. (2005) Interaction via a key tryptophan in the I-II linker of N-type calcium channels is required for beta1 but not for palmitoylated beta2, implicating

an additional binding site in the regulation of channel voltage-dependent properties. *J Neurosci* 25(30):6984–6996.
41. Kobayashi H, Fukuda M (2012) Rab35 regulates Arf6 activity through centaurin-β2 (ACAP2) during neurite outgrowth. *J Cell Sci* 125(Pt 9):2235–2243.
42. Duveau V, et al. (2011) Spatiotemporal specificity of GABAA receptor-mediated regulation of adult hippocampal neurogenesis. *Eur J Neurosci* 34(3):362–373.
43. Townsend M, Yoshii A, Mishina M, Constantine-Paton M (2003) Developmental loss of miniature N-methyl-D-aspartate receptor currents in NR2A knockout mice. *Proc Natl Acad Sci USA* 100(3):1340–1345.
44. Takahashi T, et al. (1999) Plexin-neuropilin-1 complexes form functional semaphorin-3A receptors. *Cell* 99(1):59–69.
45. Frederick AL, Saborido TP, Stanwood GD (2012) Neurobehavioral phenotyping of G (alphaq) knockout mice reveals impairments in motor functions and spatial working memory without changes in anxiety or behavioral despair. *Front Behav Neurosci* 6(article 29):1–13.
46. Swanwick CC, Shapiro ME, Vicini S, Wenthold RJ (2010) Flotillin-1 promotes formation of glutamatergic synapses in hippocampal neurons. *Dev Neurobiol* 70(13):875–883.
47. Jeon D, et al. (2003) Enhanced learning and memory in mice lacking Na+/Ca2+ exchanger 2. *Neuron* 38(6):965–976.
48. O'Sullivan ML, et al. (2012) FLRT proteins are endogenous latrophilin ligands and regulate excitatory synapse development. *Neuron* 73(5):903–910.
49. Allen D, et al. (2011) The SK2-long isoform directs synaptic localization and function of SK2-containing channels. *Nat Neurosci* 14(6):744–749.
50. Šekeljić V, Andjus PR (2012) Tenascin-C and its functions in neuronal plasticity. *Int J Biochem Cell Biol* 44(6):825–829.
51. Han S, Zhang KH, Lu PH, Xu XM (2004) Effects of annexins II and V on survival of neurons and astrocytes in vitro. *Acta Pharmacol Sin* 25(5):602–610.
52. Willard MD, et al. (2007) Selective role for RGS12 as a Ras/Raf/MEK scaffold in nerve growth factor-mediated differentiation. *EMBO J* 26(8):2029–2040.
53. Jiao S, Li Z (2011) Nonapoptotic function of BAD and BAX in long-term depression of synaptic transmission. *Neuron* 70(4):758–772.
54. Hung AY, Sung CC, Brito IL, Sheng M (2010) Degradation of postsynaptic scaffold GKAP and regulation of dendritic spine morphology by the TRIM3 ubiquitin ligase in rat hippocampal neurons. *PLoS ONE* 5(3):e9842.
55. Okuda H, Miyata S, Mori Y, Tohyama M (2007) Mouse Prickle1 and Prickle2 are expressed in postmitotic neurons and promote neurite outgrowth. *FEBS Lett* 581(24):4754–4760.
56. Huang Y, et al. (2001) CAKbeta/Pyk2 kinase is a signaling link for induction of long-term potentiation in CA1 hippocampus. *Neuron* 29(2):485–496.
57. Mandela P, Ma XM (2012) Kalirin, a key player in synapse formation, is implicated in human diseases. *Neural Plast* 2012:728161.
58. Hung AY, et al. (2008) Smaller dendritic spines, weaker synaptic transmission, but enhanced spatial learning in mice lacking Shank1. *J Neurosci* 28(7):1697–1708.
59. Carlisle HJ, Manzerra P, Marcora E, Kennedy MB (2008) SynGAP regulates steady-state and activity-dependent phosphorylation of cofilin. *J Neurosci* 28(50): 13673–13683.
60. Arikkath J (2009) Regulation of dendrite and spine morphogenesis and plasticity by catenins. *Mol Neurobiol* 40(1):46–54.
61. Abeliovich A, et al. (1993) PKC gamma mutant mice exhibit mild deficits in spatial and contextual learning. *Cell* 75(7):1263–1271.
62. Stein JM, et al. (2006) Behavioral and neurochemical alterations in mice lacking the RNA-binding protein translin. *J Neurosci* 26(8):2184–2196.
63. Lee SE, et al. (2010) RGS14 is a natural suppressor of both synaptic plasticity in CA2 neurons and hippocampal-based learning and memory. *Proc Natl Acad Sci USA* 107(39):16994–16998.
64. Chen BS, Thomas EV, Sanz-Clemente A, Roche KW (2011) NMDA receptor-dependent regulation of dendritic spine morphology by SAP102 splice variants. *J Neurosci* 31(1):89–96.
65. Cuthbert PC, et al. (2007) Synapse-associated protein 102/dlgh3 couples the NMDA receptor to specific plasticity pathways and learning strategies. *J Neurosci* 27(10): 2673–2682.
66. Liu Y, Szaro BG (2011) hnRNP K post-transcriptionally co-regulates multiple cytoskeletal genes needed for axonogenesis. *Development* 138(14):3079–3090.
67. Micheva KD, Beaulieu C (1995) An anatomical substrate for experience-dependent plasticity of the rat barrel field cortex. *Proc Natl Acad Sci USA* 92(25):11834–11838.
68. Cheng D, et al. (2006) Relative and absolute quantification of postsynaptic density proteome isolated from rat forebrain and cerebellum. *Mol Cell Proteomics* 5(6): 1158–1170.
69. Barnett MW, et al. (2006) Synaptic Ras GTPase activating protein regulates pattern formation in the trigeminal system of mice. *J Neurosci* 26(5):1355–1365.
70. Clement JP, et al. (2012) Pathogenic SYNGAP1 mutations impair cognitive development by disrupting maturation of dendritic spine synapses. *Cell* 151(4):709–723.
71. Shim SY, et al. (2008) Protein 600 is a microtubule/endoplasmic reticulum-associated protein in CNS neurons. *J Neurosci* 28(14):3604–3614.
72. Lin A, et al. (2011) Nedd4-mediated AMPA receptor ubiquitination regulates receptor turnover and trafficking. *J Neurochem* 119(1):27–39.
73. Brown MW, Horn G (1990) Are specific proteins implicated in the learning process of imprinting? *Brain Res Dev Brain Res* 52(1–2):294–297.
74. Liao L, et al. (2007) BDNF induces widespread changes in synaptic protein content and up-regulates components of the translation machinery: An analysis using high-throughput proteomics. *J Proteome Res* 6(3):1059–1071.
75. Liao L, McClatchy DB, Yates JR (2009) Shotgun proteomics in neuroscience. *Neuron* 63(1):12–26.
76. O'Rourke NA, Weiler NC, Micheva KD, Smith SJ (2012) Deep molecular diversity of mammalian synapses: Why it matters and how to measure it. *Nat Rev Neurosci* 13(6): 365–379.
77. Cheetham CE, Barnes SJ, Albieri G, Knott GW, Finnerty GT (2012) Pansynaptic enlargement at adult cortical connections strengthened by experience. *Cereb Cortex*.
78. Micheva KD, Beaulieu C (1997) Development and plasticity of the inhibitory neocortical circuitry with an emphasis on the rodent barrel field cortex: A review. *Can J Physiol Pharmacol* 75(5):470–478.
79. Miyazaki T, et al. (2012) Developmental AMPA receptor subunit specificity during experience-driven synaptic plasticity in the rat barrel cortex. *Brain Res* 1435:1–7.
80. Keck T, et al. (2011) Loss of sensory input causes rapid structural changes of inhibitory neurons in adult mouse visual cortex. *Neuron* 71(5):869–882.
81. van Versendaal D, et al. (2012) Elimination of inhibitory synapses is a major component of adult ocular dominance plasticity. *Neuron* 74(2):374–383.
82. Zuo Y, Yang G, Kwon E, Gan WB (2005) Long-term sensory deprivation prevents dendritic spine loss in primary somatosensory cortex. *Nature* 436(7048):261–265.
83. Hamdan FF, et al. (2011) De novo SYNGAP1 mutations in nonsyndromic intellectual disability and autism. *Biol Psychiatry* 69(9):898–901.
84. Muhia M, Yee BK, Feldon J, Markopoulos F, Knuesel I (2010) Disruption of hippocampus-regulated behavioural and cognitive processes by heterozygous constitutive deletion of SynGAP. *Eur J Neurosci* 31(3):529–543.
85. Diez-Roux G, et al. (2011) A high-resolution anatomical atlas of the transcriptome in the mouse embryo. *PLoS Biol* 9(1):e1000582.
86. Hong W, Mosca TJ, Luo L (2012) Teneurins instruct synaptic partner matching in an olfactory map. *Nature* 484(7393):201–207.
87. Silva JP, et al. (2011) Latrophilin 1 and its endogenous ligand Lasso/teneurin-2 form a high-affinity transsynaptic receptor pair with signaling capabilities. *Proc Natl Acad Sci USA* 108(29):12113–12118.
88. Schwarz LA, Hall BJ, Patrick GN (2010) Activity-dependent ubiquitination of GluA1 mediates a distinct AMPA receptor endocytosis and sorting pathway. *J Neurosci* 30(49):16718–16729.
89. Feldman DE (2009) Synaptic mechanisms for plasticity in neocortex. *Annu Rev Neurosci* 32:33–55.
90. Sacktor TC (2011) How does PKMζ maintain long-term memory? *Nat Rev Neurosci* 12(1):9–15.
91. Kandel ER (2012) The molecular biology of memory: cAMP, PKA, CRE, CREB-1, CREB-2, and CPEB. *Mol Brain* 5(1):14.
92. Cajigas IJ, et al. (2012) The local transcriptome in the synaptic neuropil revealed by deep sequencing and high-resolution imaging. *Neuron* 74(3):453–466.
93. Maier T, Güell M, Serrano L (2009) Correlation of mRNA and protein in complex biological samples. *FEBS Lett* 583(24):3966–3973.
94. Dahlhaus M, et al. (2011) The synaptic proteome during development and plasticity of the mouse visual cortex. *Mol Cell Proteomics* 10(5):M110 005413.
95. Jacob V, Petreanu L, Wright N, Svoboda K, Fox K (2012) Regular spiking and intrinsic bursting pyramidal cells show orthogonal forms of experience-dependent plasticity in layer V of barrel cortex. *Neuron* 73(2):391–404.
96. Butko MT, et al. (2012) Fluorescent and photo-oxidizing TimeSTAMP tags track protein fates in light and electron microscopy. *Nat Neurosci* 15(12):1742–1751.
97. De Jaco A, et al. (2010) Neuroligin trafficking deficiencies arising from mutations in the alpha/beta-hydrolase fold protein family. *J Biol Chem* 285(37):28674–28682.
98. Lin MZ, Glenn JS, Tsien RY (2008) A drug-controllable tag for visualizing newly synthesized proteins in cells and whole animals. *Proc Natl Acad Sci USA* 105(22): 7744–7749.
99. McClatchy DB, Dong MQ, Wu CC, Venable JD, Yates JR, 3rd (2007) 15N metabolic labeling of mammalian tissue with slow protein turnover. *J Proteome Res* 6(5):2005–2010.
100. MacCoss MJ, Wu CC, Matthews DE, Yates JR, 3rd (2005) Measurement of the isotope enrichment of stable isotope-labeled proteins using high-resolution mass spectra of peptides. *Anal Chem* 77(23):7646–7653.
101. Link AJ, et al. (1999) Direct analysis of protein complexes using mass spectrometry. *Nat Biotechnol* 17(7):676–682.
102. Washburn MP, Wolters D, Yates JR, 3rd (2001) Large-scale analysis of the yeast proteome by multidimensional protein identification technology. *Nat Biotechnol* 19(3):242–247.
103. McDonald WH, et al. (2004) MS1, MS2, and SQT-three unified, compact, and easily parsed file formats for the storage of shotgun proteomic spectra and identifications. *Rapid Commun Mass Spectrom* 18(18):2162–2168.
104. Peng J, Elias JE, Thoreen CC, Licklider LJ, Gygi SP (2003) Evaluation of multidimensional chromatography coupled with tandem mass spectrometry (LC/LC-MS/MS) for large-scale protein analysis: The yeast proteome. *J Proteome Res* 2(1):43–50.
105. Xu T, et al. (2006) ProLuCID, a fast and sensitive tandem mass spectra-based protein identification program. *Mol Cell Proteomics* 5(10):S174–S174.
106. Cociorva D, Tabb DL, Yates JR (2007) Validation of tandem mass spectrometry database search results using DTASelect. *Current Protocols in Bioinformatics* eds Andreas D. Baxevanis AD, et al. (John Wiley & Sons, Inc., Hoboken, NJ), Chapter 13:Unit 13–14.
107. Tabb DL, McDonald WH, Yates JR, 3rd (2002) DTASelect and Contrast: Tools for assembling and comparing protein identifications from shotgun proteomics. *J Proteome Res* 1(1):21–26.
108. Eng JK, Mccormack AL, Yates JR (1994) An approach to correlate tandem mass-spectral data of peptides with amino-acid-sequences in a protein database. *J Am Soc Mass Spectrom* 5(11):976–989.
109. Park SK, Venable JD, Xu T, Liao L, Yates JR (2006) A tool for quantitative analysis of high-throughput mass spectrometry data. *Mol Cell Proteomics* 5(10):S199–S199.
110. Sosinsky GE, et al. (2008) The combination of chemical fixation procedures with high pressure freezing and freeze substitution preserves highly labile tissue ultrastructure for electron tomography applications. *J Struct Biol* 161(3):359–371.